



# High-Performance Aqueous Zinc-Ion Battery Based on Laser-Induced Graphene

Chengjuan Yang<sup>1,2</sup> · Yuchun Tong<sup>1,2</sup> · Zhen Yang<sup>1,2</sup> · Hui Xiao<sup>1,2</sup> · Huimin Qi<sup>1,2</sup> · Faze Chen<sup>1,2</sup>

Received: 21 December 2022 / Revised: 23 March 2023 / Accepted: 27 March 2023  
© The Author(s) 2023

## Abstract

Zn-ion batteries (ZIBs) have a broad application prospect because of their advantages of high power, large capacity, and high energy density. However, the development of high-capacity, long-lifespan ZIBs is challenging because of the faster dendrite growth and the occurrence of the hydrogen evolution reaction. Laser-induced graphene (LIG) is a material with many defects and heteroatoms. Because of these characteristics, it plays an important role in improving nucleation. A simple and effective method for preparing LIG was proposed in this paper, and the LIG was covered on the surface of Zn foil to form a composite structure. This structure substantially reduces the nucleation overpotential of Zn and slows down the dendrite growth of Zn by improving the nucleation behavior of  $Zn^{2+}$ . Simultaneously, the three-dimensional porous structure increases the specific surface area of the electrode, so the battery has a larger specific capacity. Compared with the bare Zn electrode, the composite electrode possesses lower overpotential and longer cycle life. In addition, the full battery using activated carbon as the active material exhibits great rate and cycle performance. This facile and scalable approach may solve the problem of Zn dendrite growth, which is crucial for the large-scale application of ZIBs.

## Highlights

1. The application of laser-induced graphene on zinc anode effectively prolongs the lifespan of Zn batteries.
2. A three-dimensional structure was constructed on Zn foil surface, significantly increasing the capacity of the Zn battery.
3. The important role of laser-induced graphene in promoting zinc nucleation was demonstrated.

**Keywords** Laser-induced graphene · Zinc-ion batteries · Dendrite · Femtosecond laser

✉ Zhen Yang  
yangzhen1992@tju.edu.cn

Chengjuan Yang  
cyjtu@tju.edu.cn

Yuchun Tong  
tyc\_rl@tju.edu.cn

<sup>1</sup> School of Mechanical Engineering, Tianjin University, Tianjin 300354, China

<sup>2</sup> Key Laboratory of Mechanism Theory and Equipment Design of Ministry of Education, Tianjin 300072, China

## 1 Introduction

Recently, renewable energy technology has been developed vigorously, which has stimulated the development of energy storage devices. Increasingly more attention has been paid to the research of green, low-cost, and safe energy storage systems. Lithium-ion batteries (LIBs) are widely used in vehicle and convenient energy storage applications because of their high power, high energy, and long cycle life [1–3]. However, some disadvantages of LIBs, such as high cost, poor security, and scarcity of lithium resources, limit their large-scale application in energy storage devices. Therefore, cheaper and safer energy storage systems must be developed.

Compared with organic electrolytes, water electrolytes have the advantages of nonflammability and low cost. Recently, aqueous Zn-ion batteries (ZIBs) have attracted considerable attention because of their superior performance. Aqueous Zn-based batteries include zinc-air batteries, nickel-zinc batteries, and zinc-manganese batteries [4–7]. Zinc is recognized as the most promising anode material after lithium. This promise is mainly attributed to the advantages provided by zinc, including low oxidation–reduction potential ( $-0.762$  V), high theoretical capacity ( $820 \text{ mA hg}^{-1}$ ), low cost, and stable properties in air [8–11]. These attributes make ZIBs potentially commercially viable on a large scale. Although zinc has many advantages as a metal anode, some intractable challenges hinder the large-scale application of ZIBs. The main problem is the instability of the zinc anode during cycling [12, 13]. Because of an uneven charge distribution on the zinc surface, the nonuniform zinc-ion flux driven by the tip effect usually leads to the uneven nucleation and growth of zinc dendrites. This result can lead to short circuits at the micro-scale and even battery failure. In addition, in the negative electrode reaction, zinc will be lost and produce by-products due to side reactions, which further leads to a decrease in Coulomb efficiency (CE) and lifespan [14].

To solve the problem of the growth of zinc dendrites, many innovative strategies have been reported. Bayaguud et al. [15] proposed low-cost, nontoxic, tetrabromobutyl ammonium sulfate ( $\text{TBA}_2\text{SO}_4$ ) as an electrolyte additive. In the process of galvanizing,  $\text{TBA}^+$  ions adsorbed on the negative surface of zinc metal regulated the initial nuclear potential, inhibited the growth of dendrites by shielding the hydrated zinc ions in the electrolyte, and induced the uniform deposition of zinc metal on the commercial copper foam (Cu) matrix. In addition, the preparation of a three-dimensional structure on the surface of zinc foil is also a common method for improving the performance of a zinc anode. The introduction of a nonuniform porous passivation layer on a zinc anode is an effective method for achieving uniform zinc electrodeposition [16, 17]. High current density can promote dendrite nucleation, and a three-dimensional structure can reduce effective current density and promote ion diffusion, which is conducive to zinc deposition [18, 19]. For example, Kang et al. [20] adopted a chemically corroded porous copper skeleton as a fluid collector. A three-dimensional porous copper skeleton has great electrical conductivity and an open structure, which is conducive to uniform deposition/stripping of zinc. Nevertheless, battery performance is still difficult to improve in the existing ways. The stable cycle of a zinc anode under the actual capacity still needs to be studied. The development of ZIBs needs to be further promoted by a high-area-capacity zinc anode that is manufactured by an expandable and simple manufacturing method.

Graphene as a modified coating has often been used as an energy storage material [21, 22]. Recently, an alternative method for manufacturing carbon-based materials has attracted great attention because of its ease of scalability, high tunability, and cost-effectiveness [23]. Polymer materials such as polyimide (PI) and polyester can immediately be carbonized into a wide range of carbon-based materials by direct laser marking. The most famous example of this carbonization process is laser-induced graphene (LIG) [24]. Because the structure and composition of LIG are adjustable, such materials have been used as catalysts, supercapacitors, and sensors [25–27]. Notably the characteristics of LIG are high porosity, high electrochemical stability, relatively good electron conductivity, and multidoping properties [28]. These characteristics meet the basic requirements of an ideal electric collector.

In this study, a laser was used to scribe on a PI film covered on Zn foil to generate a 3D composite structure containing LIG. The nucleation overpotential of zinc on the Zn foil containing LIG was considerably lower than that on the bare Zn foil. There was even no nucleation barrier at low current density. The LIG in the groove can guide the uniform deposition of  $\text{Zn}^{2+}$  in this structure, and Zn dendrite formation was effectively inhibited. In addition, the 3D porous structure formed by laser irradiation enhanced the hydrophilicity of the Zn surface. This result benefited the material exchange of  $\text{Zn}^{2+}$  in an aqueous electrolyte. LIG-Zn stable overvoltage could be maintained during the cycle, and the cycle life was substantially increased ( $> 600$  h at  $1 \text{ mA cm}^{-2}$ ). In the supercapacitors using activated carbon (AC) as the cathode, the LIG-Zn anode exhibited better cycle stability.

## 2 Experimental Section

### 2.1 Preparation of the LIG-Zn Anode

The preparation process of the LIG-Zn sample is schematized in Fig. 1. Commercial Zn foil was ultrasonically cleaned using acetone, ethanol, and deionized water to eliminate residual organic matter from the surface prior to preparation. Commercial Kapton tape (polyimide, PI) was attached to the Zn foil and then processed with a femtosecond laser. The thickness of the Zn foil was  $100 \mu\text{m}$ , while that of the Kapton tape was  $60 \mu\text{m}$ . PI was converted to LIG after laser irradiation. Two processes occur simultaneously, namely, the graphitization of PI and the ablation of materials. Therefore, the balance of these two processes must be ensured. Higher-quality LIG was generated by adjusting the scanning rate and energy density of the laser. A femtosecond laser with a wavelength of  $1064 \text{ nm}$ , a pulse width

**Fig. 1** Schematic of the preparation process of LIG-Zn

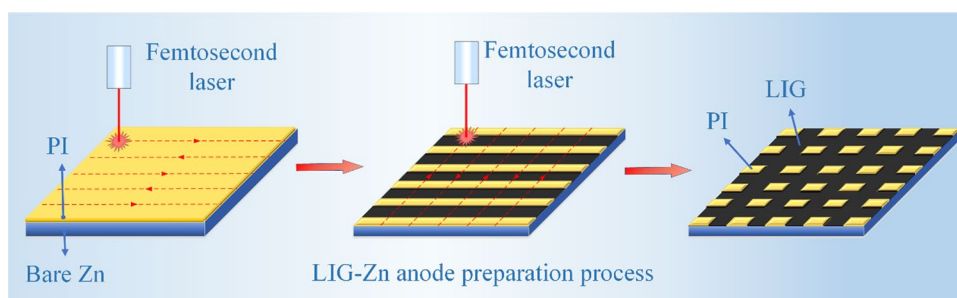
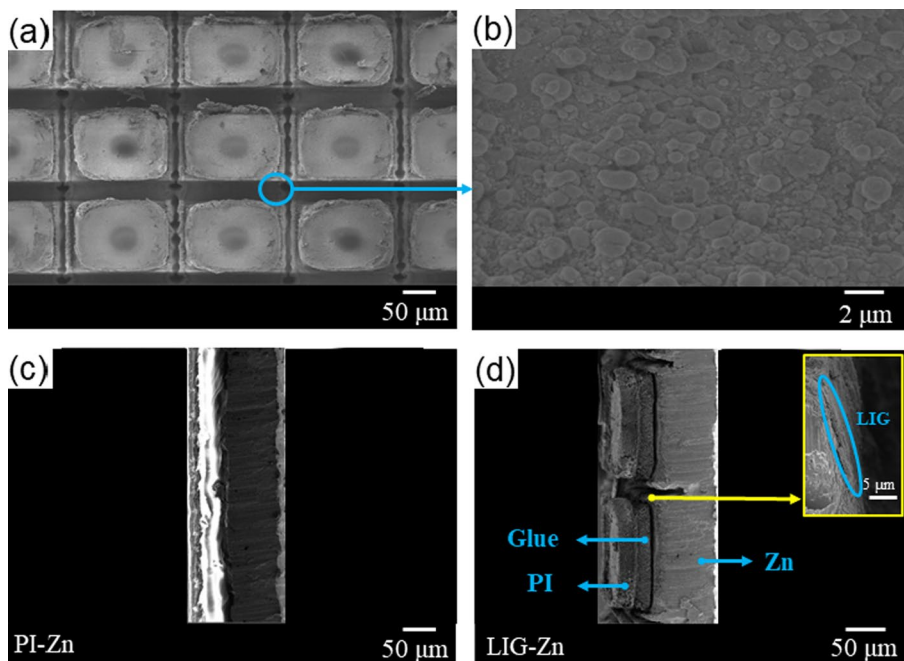


**Fig. 2** SEM images of **a, b** a schematic of the structure of LIG-Zn; and **c, d** sectional drawing before and after laser processing



of 340 fs, and a repetition frequency of up to 50 kHz was used for processing. The laser fluence at the focal point was  $F = 5.94 \text{ J cm}^{-2}$ . The laser performs raster scanning at a scanning interval of  $100 \mu\text{m}$  and a scanning speed of  $200 \text{ mm s}^{-1}$ . After processing, a periodic concave-convex pattern on the microscale was generated on the surface of the sample, as shown in Fig. 2a.

## 2.2 Material Characterization

The surface microstructure of the treated sample was observed using scanning electron microscopy (SEM). The chemical composition of the surface was characterized using X-ray photoelectron spectroscopy (XPS). The crystal structure was characterized using X-ray diffraction (XRD) spectroscopy.

## 2.3 Preparation of the AC Cathode

AC was used as the cathode active material for full cell testing. The preparation method was as follows: The paste was prepared by mixing AC powder, polyvinylidene fluoride, and carbon black (8:1:1) in 1-methyl-2-pyrrolidone solvent. Then this paste was coated on stainless steel. Finally, the electrode was dried at  $110 \text{ }^\circ\text{C}$  for 12 h in a vacuum to complete the preparation of the AC cathode electrode.

## 2.4 Electrochemical Measurements

Electrochemical tests were performed at room temperature. The standard 8-channel *LAND* battery test system was used to test battery performance. LIG-Zn and Zn electrodes were assembled into a 2025 button battery for

electrochemical measurement. The electrolyte was 2 mol/L  $\text{ZnSO}_4$  aqueous solution, and the amount of electrolyte in each battery was 100  $\mu\text{L}$ . A glass fiber was used as a battery diaphragm. To investigate the electrochemical behavior of Zn, a constant current charge–discharge cycle of the symmetric battery was performed at a current density of 1–4  $\text{mA cm}^{-2}$  and a total capacity of 0.5–2  $\text{mAh cm}^{-2}$ . The CE and electroplating stripping curve were tested using a smooth copper foil as the positive electrode.

To perform the electrochemical test of the zinc-ion hybrid supercapacitor, a button battery was assembled with AC as the cathode material and bare Zn and LIG-Zn as the anode. The test voltage was 0.2–1.8 V. Additionally, the specific capacity was calculated according to the quality of AC to clearly explain the improvement in battery performance.

The charge transfer resistance of the negative electrode was evaluated using an electrochemical workstation (PGSTAT302 N, Metrohm, Switzerland). Electrochemical impedance spectroscopy (EIS) experiments were performed in the range of scanning frequencies from  $10^{-2}$  to  $10^5$  Hz, and the sinusoidal potential perturbation was 10 mV rms. Each test was repeated more than five times to verify the repeatability of the results.

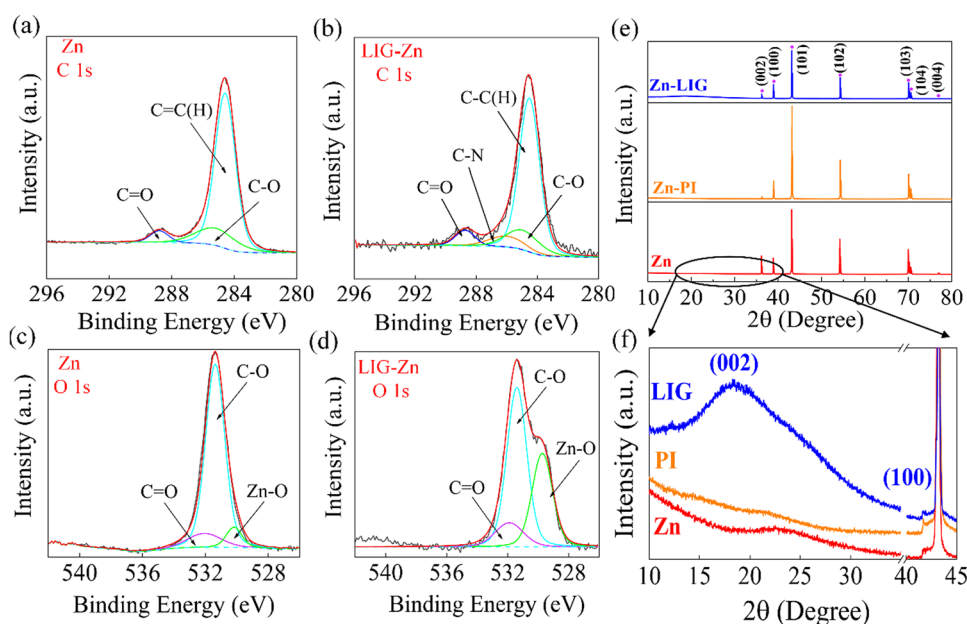
### 3 Results and Discussion

The microstructure of the prepared LIG-Zn anode is shown in Fig. 2a. Under laser irradiation, some of the PI films blackened and deposited in the groove, indicating that it was converted to graphene. The PI band was completely cut to

form a columnar structure with clear layers. The unablated PI film was attached to the surface of the Zn column, while the porous graphene layer covered the bottom of the tank and the side wall of the Zn column. Figure 2b clearly shows the microstructure of LIG, which contains many defects. This porous structure can lead to a more uniform deposition of  $\text{Zn}^{2+}$ . The section is shown in Fig. 2c and d. After laser processing, the Zn foil can be divided into three structures: Zn substrate, LIG in the slot, and PI film on the array column. Figure 2d shows that the LIG was approximately 1  $\mu\text{m}$  thick, covering the groove bottom and the sidewalls.

To further study the properties of LIG, XPS tests on LIG-Zn and bare Zn samples were performed for the deconvolution of C 1s and O 1s spectra (Fig. 3a–d). For bare Zn samples, C 1s mainly produces C–C, C–O, and C=O peaks at approximately 284.6, 285, and 288.2 eV, respectively. This result is due to the presence of organic matter in the air, which was attached to the Zn surface. For LIG-Zn, C–N appears at 285.4 eV after laser irradiation [29]. PI might be a nitrogen source, and some nitrogen remained on the surface of Zn after laser processing. In addition, a C–N peak appeared in the spectrum of N 1s. However, further deconvolution of the N 1s peak with relatively low intensity did not yield reliable results. In addition, the Zn–O peak appeared at 529.6 eV. The reaction between the Zn substrate and  $\text{O}_2$  generates ZnO on the surface of the bare Zn substrate through a high-energy laser. The surface of zinc foil can be more hydrophilic because of the effect of ZnO, and the deposition kinetics of Zn can inhibit the hydrogen evolution reaction and improve the cycle life of the battery [30, 31]. According to the characteristic peaks of the O 1s and C 1s spectra, the

**Fig. 3** a, b C 1s XPS spectra of bare Zn and LIG-Zn; c, d O 1s XPS spectra of bare Zn and LIG-Zn; and e, f XRD patterns of bare Zn, PI-coated Zn foil and LIG-Zn



content of C=O in LIG-Zn was higher. This result might be caused by the porous structure, multidefects, and multidoping properties of LIG. This special structure benefits the nucleation of Zn. An XRD spectroscopy was employed to characterize the composition of bare Zn, PI-coated Zn foil, and LIG-Zn (Fig. 3e). The typical peaks of Zn appear in the XRD images of the three samples. In Zn-PI and Zn-LIG, the intensity of the characteristic peak at (002) was obviously decreased, which is because the surface of the Zn foil was covered by insulating PI after processing, and zinc ions tended to be deposited in the groove. As shown in Fig. 3f, the (002) characteristic peak of LIG appears near  $20^\circ$ , which proves the generation of LIG after laser processing [32].

To clearly show the influence of LIG-Zn on the deposition behavior of zinc ions, the surface morphology of electrodes with different deposition capacities was studied, as shown in Fig. 4. The deposition behavior of LIG-Zn and bare Zn foil anodes was examined using a vertical view of SEM. An aqueous solution of  $\text{ZnSO}_4$  (2 M) was used as the electrolyte. A constant current of  $1 \text{ mA cm}^{-2}$  was used to deposit different capacities on the anode. The surface morphology of the electrode after deposition for 1, 5, 10, and 20 h was studied. After 1 h of deposition at a current density of  $1 \text{ mA cm}^{-2}$ , numerous thin sheets were formed on the initially smooth surface of Zn (Fig. 4e). The dimensions of these vertical and sharp flakes are approximately  $5 \mu\text{m}$ . The accumulation of electric charge further accelerates the growth of dendrites, which makes the dendrites larger and sharper. As shown in Fig. 4h, when the deposition time increases to 20 h, many dendrites gather on the Zn foil, forming an uneven plane or

even piercing the separator, which results in a short circuit of the battery. In contrast, Zn was mainly deposited in the grooves in the LIG-Zn anode. The uniform deposition of Zn in the LIG can be clearly observed. Figure 4a–d shows that Zn was laterally deposited on the LIG-Zn anode. There was no vertical dendritic process but a dense arrangement of scale-like structures. Even after 20 h of electroplating, no larger dendrite was obtained. These results showed that LIG formation could effectively inhibit the growth and evolution of Zn dendrites. The width and depth of the LIG-Zn anode groove affect the maximum capacity of the electrode. Thus, the theoretical capacity of the electrode could be predicted by describing the volume of the groove. The electrode reaches the theoretical capacity when Zn fills the gap between PI columns. Then, Zn begins to be deposited on the surface of the LIG-Zn rather than inside, substantially reducing battery performance. Therefore, the requirement of actual capacity was often an important factor to be considered.

A symmetrical LIG-Zn||LIG-Zn battery and bare Zn||Zn battery were prepared with 2 M  $\text{ZnSO}_4$  electrolyte to test their electrochemical performance. Figure 5a shows the initial electroplating overpotential distribution of the symmetrical battery at  $1 \text{ mA cm}^{-2}$ . In this image, the difference between the peak overpotential and the subsequent stable plating overpotential indicates the nucleation overpotential [33, 34]. As shown in Fig. 5a, at a current density of  $1 \text{ mA cm}^{-2}$ , LIG-Zn and bare Zn had nucleation overpotentials of 2.8 and 35 mV, respectively. This comparison suggests that adding LIG activated the Zn nucleation process and reduced the Zn deposition resistance during the first

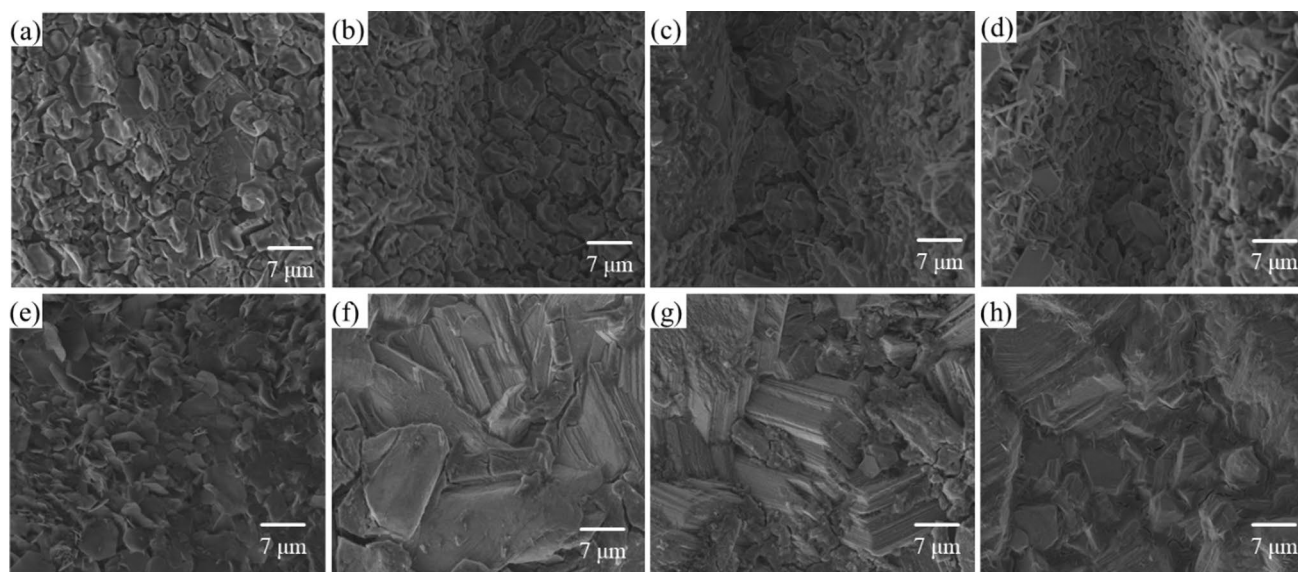


**Fig. 4** SEM images of deposition morphologies at different deposition times. SEM image of Zn deposition for **a** 1 h, **b** 5 h, **c** 10 h, and **d** 20 h on LIG-Zn and **e** 1 h, **f** 5 h, **g** 10 h, and **h** 20 h on bare Zn foil at a current density of  $1 \text{ mA cm}^{-2}$

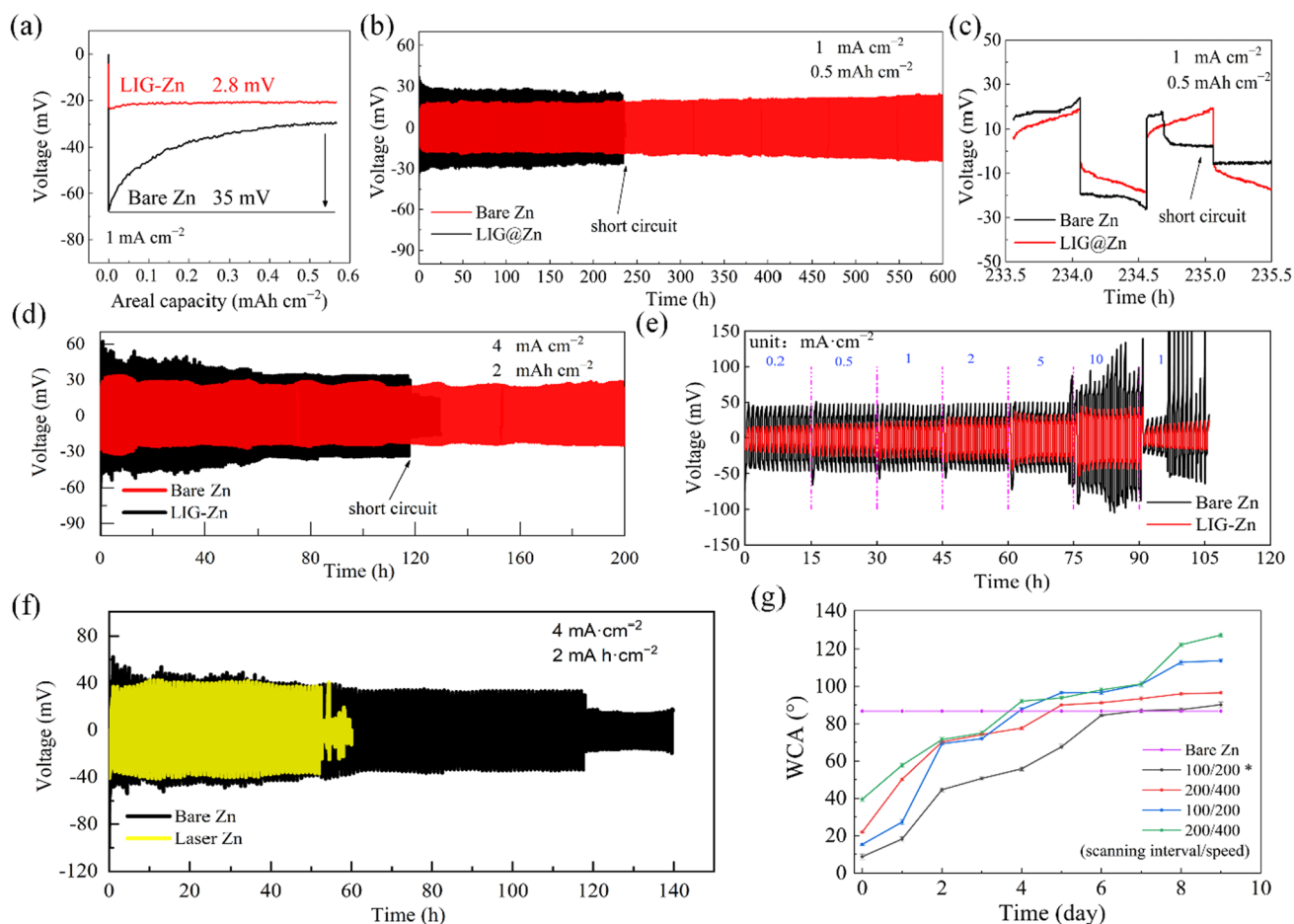


**Fig. 5** Symmetrical battery test. **a** Initial plating voltage profiles of LIG-Zn and bare Zn, tested in symmetrical cells at  $1 \text{ mA cm}^{-2}$ ; **b**, **c** voltage profiles tested at  $1 \text{ mA cm}^{-2}$  with  $0.5 \text{ mA h cm}^{-2}$  capacity per cycle; **d** voltage profiles tested at  $4 \text{ mA cm}^{-2}$  with  $2 \text{ mA h cm}^{-2}$  capacity per cycle; **e** rate property of symmetrical cells at current

densities of 0.2, 0.5, 1, 2, 5, 10, and  $1 \text{ mA cm}^{-2}$ ; **f** voltage profiles tested on a bare Zn electrode and laser processed Zn electrodes at  $4 \text{ mA cm}^{-2}$  with  $2 \text{ mA h cm}^{-2}$  capacity per cycle; and **g** the transformation of the water contact angle on the surface of Zn foil under different laser parameters

cycle, making it easier for LIG-Zn to enter the stable grain growth stage. The reduction of the Zn nucleation barrier promoted the formation of small Zn nuclei on the electrode rather than the rapid growth of disordered Zn dendrites. The repeated electroplating/stripping properties of LIG-Zn and bare Zn were evaluated using constant current cycling at different current densities and capacities. Figure 5b shows the constant current cycle performance of a symmetrical cell with an areal capacity of  $0.5 \text{ mA h cm}^{-2}$  at a current density of  $1 \text{ mA cm}^{-2}$ . For the bare Zn-based batteries, the voltage fluctuation and polarization were obvious. The voltage drops suddenly at 234 h, indicating a short circuit of the battery. This short circuit occurred because numerous sharp and large blocks of Zn dendrites were formed in the long-term cycle, which eventually penetrated the separator and led to a short circuit inside the battery. As shown in Fig. 5c, short-circuit failure was manifested as perfect rectangular voltage profiles with constant minuscule overpotential

corresponding to the ohmic loss in the electrically conductive zinc. In contrast, LIG-Zn has stable electroplating/stripping polarization, and the cycle time can be more than 600 h. Figure 5d shows the cycle performance of the battery at a higher current density of  $4 \text{ mA cm}^{-2}$ . The battery with a bare Zn electrode was short-circuited after 120 h, while the LIG-Zn battery could maintain a stable cycle for more than 200 h. During the cycle, the LIG-Zn battery showed a stable polarization voltage of approximately 30 mV, and there was no electrochemical evidence of a transient short circuit. To further understand the electroplating/stripping kinetics, the voltage polarization was analyzed at different current densities. Figure 5e shows the rate performance of the battery at current densities of 0.2–10  $\text{mA cm}^{-2}$ . LIG-Zn obviously has a small polarization in each current density cycle. The voltage of the Zn||Zn symmetrical battery increased substantially with increasing current density and finally failed after the electrochemical test of  $10 \text{ mA cm}^{-2}$ . The mean

overpotential values for the bare Zn cell were 43.5, 48.6, 50.1, 52.3, and 85.7 mV at 0.2, 0.5, 1, 2, 5, and 10 mA cm<sup>-2</sup>, respectively. In contrast, the LIG-Zn symmetrical battery showed a highly reversible zinc deposition/exfoliation curve during the test. The polarization voltage remained stable after the 10 mA cm<sup>-2</sup> current cycle. The average plating/stripping overpotentials were 16.7, 19.5, 22.3, 27.5, and 36.2 mV when tested at 0.2, 0.5, 1, 2, 5, and 10 mA cm<sup>-2</sup>, respectively. According to the literature report, the higher the overpotential of the electrode, the more difficult nucleation will be, which leads to increased polarization, poor CE, electrode damage, and even battery failure [35]. The low polarization and stable voltage distribution of the LIG anode were beneficial for guiding the nucleation of zinc and achieving a dendrite-free zinc anode during uniform deposition [16, 36, 37].

In the experiment, the three-dimensional porous structure formed only by laser processing was noticed to also influence battery performance. Therefore, a set of control experiments was added to explore the mechanism of the effect of laser irradiation on the Zn anode. The constant current cycle diagrams of the batteries with a bare Zn anode and laser-processed Zn anode at a current density of 4 mA cm<sup>-2</sup> and an areal capacity of 2 mAh cm<sup>-2</sup> are shown in Fig. 5f. Although the laser Zn anode has a low overpotential in the initial cycling, a short circuit occurs after only 50 h. Its cycle performance was even inferior to those of batteries with bare Zn electrodes. Figure 5g shows the change in the

water contact angle (WCA) on the surface of the Zn foil with time under different laser parameters. The WCA of Zn foil that had just been processed by a laser was near 0°, and the surface was super-hydrophilic. This hydrophilic surface increases the contact area between the Zn<sup>2+</sup> in the aqueous electrolyte and the electrode such that the zinc ions are more uniformly deposited on the surface of the Zn electrode. However, the original hydrophilic surface of Zn foil gradually transforms into a hydrophobic surface due to the dark environment in the battery with increasing time [38]. The hydrophobic surface makes zinc ions more inclined to gather and deposit, intensifying Zn dendrite formation. This time-dependent wettability was not conducive to stable battery operation. Therefore, the addition of LIG stabilized the deposition behavior of zinc ions. The Zn dendrite growth was inhibited.

LIG-Zn||Cu and bare Zn||Cu half-cells were used to test the CE. As shown in Fig. 6a, Zn plating was performed at a current of 4 mA cm<sup>-2</sup> for 0.5 h. Accordingly, Zn stripping was performed at a cutoff potential of 0.5 V at 4 mA cm<sup>-2</sup>. The stability of the battery using bare Zn as an anode decreased considerably after 80 cycles, showing that CE deteriorated rapidly. Correspondingly, when the LIG-Zn battery showed excellent cycle stability during the 300th electroplating/stripping cycle, and the average CE was maintained at 99.8%. As shown in Fig. 6b, the LIG-Zn battery could stably cycle more than 100 times even at a low voltage of 1 mA cm<sup>-2</sup>, while the bare Zn electrodes failed after

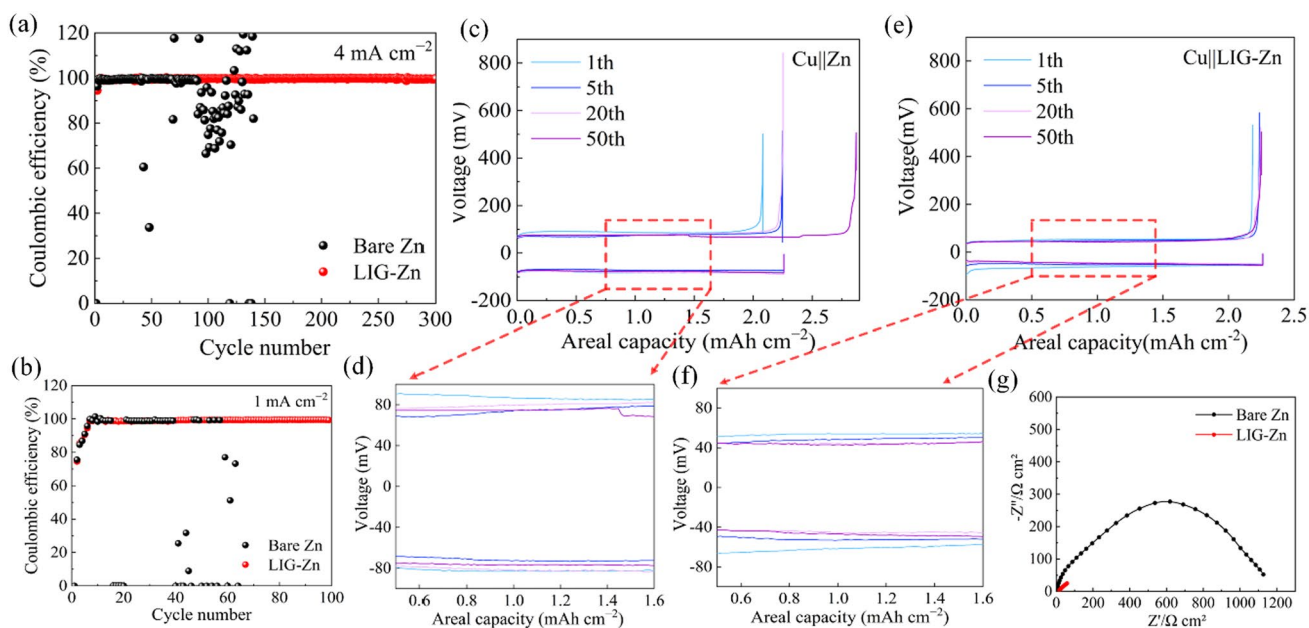


**Fig. 6** **a** Coulombic efficiency (CE) of LIG-Zn||Cu and bare Zn||Cu, tested at 4 mA cm<sup>-2</sup> with a plating areal capacity of 2 mA h cm<sup>-2</sup>; **b** CE of the plating/stripping of LIG-Zn||Cu and bare Zn||Cu cells at a capacity of 1 mAh cm<sup>-2</sup> and a current density of 1 mA cm<sup>-2</sup>; **c**,

**d** associated voltage profiles of the half-cells of LIG-Zn||Cu and bare Zn||Cu, tested at 4 mA cm<sup>-2</sup> with a plating areal capacity of 2 mA h cm<sup>-2</sup>; and **g** EIS Nyquist plots of the two specimens before cycling

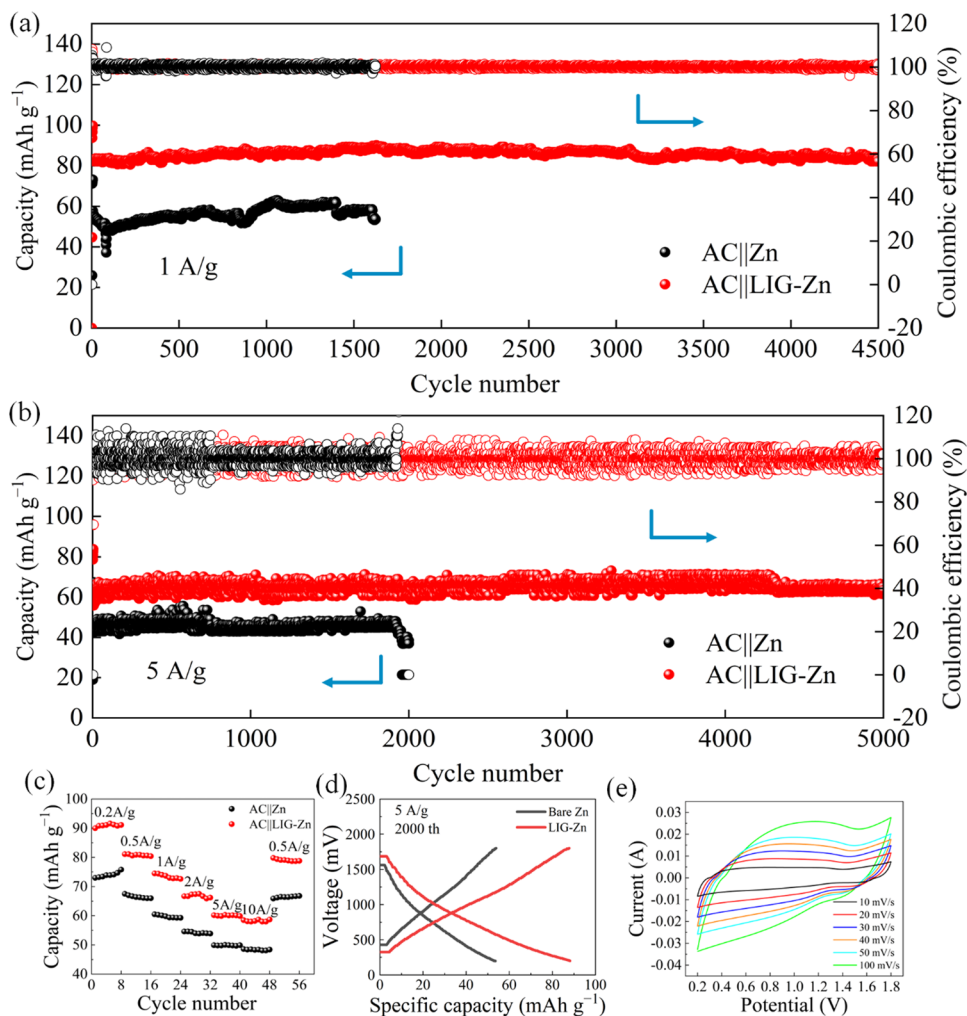
only 40 cycles. Figure 6c–f show the plating/stripping curves of bare Zn and LIG-Zn at a current density of  $4 \text{ mA cm}^{-2}$ , respectively, at the 1st, 5th, 20th, and 50th cycles. For the LIG-Zn||Cu cell, the Zn deposition potential was only  $-59 \text{ mV}$ , and the dissolution potential was  $52 \text{ mV}$  in the first cycle. The potential of Zn deposition and dissolution remained almost the same even after 50 cycles. However, for the Zn||Cu battery, the overpotential of Zn increased substantially with an increase in the number of cycles during electroplating and stripping. In the 50th cycle, the Zn deposition potential was  $-80 \text{ mV}$ , and the dissolution potential was  $90 \text{ mV}$ . This phenomenon might be due to the special structure of LIG. LIG was highly porous, and its surface area was much larger than that of the bare Zn foil. Therefore, the local current density of LIG-Zn in the process of Zn deposition was much lower than that on the bare Zn foil. Thus, lower nucleation overpotential and deposition potential were achieved on the LIG-Zn anode. Because Zn is easier to strip at lower deposition potential, LIG-Zn has high cycle stability and CE. In addition, elements such as N and O with defects also have a certain adsorption effect on Zn [39]. This effect

might be a reason why LIG more readily plated/stripped Zn from the Zn foil surface.

Figure 6g shows the EIS of the electrode in the original state. The test frequency range was  $100.00\text{--}0.01 \text{ Hz}$ . The deletion of Warburg resistance was consistent with the literature [40]. The charge transfer resistance of the symmetrical battery was considerably lower on LIG-Zn than on bare Zn. This decrease in charge transfer resistance was due to hydrophilic surface formation after laser processing [41]. The lower charge transfer resistance benefited the transfer and nucleation of zinc ions.

To further prove the excellent performance of LIG, AC material was used as the cathode to make the full battery for testing. The AC||LIG-Zn battery and AC||Zn coin battery were circulated at currents of  $1 \text{ A g}^{-1}$  and  $5 \text{ A g}^{-1}$  to obtain the change trends of CE and discharge capacity with the number of cycles. As shown in Fig. 7a, LIG-Zn had a high specific discharge capacity of  $80 \text{ mAh g}^{-1}$  in the initial cycle. The initial discharge-specific capacity of the corresponding bare Zn battery was only  $50.3 \text{ mAh g}^{-1}$ . After 4000 cycles, the capacity of the battery was  $78.7 \text{ mAh g}^{-1}$ ,

**Fig. 7** Electrochemical performance of LIG-Zn||AC and bare Zn||AC full cells. **a** Cycling performance at  $1 \text{ A g}^{-1}$ ; **b** cycling performance at  $5 \text{ A g}^{-1}$ ; **c** rate capability at different current densities; **d** 2000th cycle charging/discharging profiles of the two cells at  $5 \text{ A g}^{-1}$ ; and **e** CV curves of AC||LIG-Zn cells at various scan rates





with a high-capacity retention rate of more than 90%. The CE of the AC||LIG-Zn battery was maintained at 99.9%. In contrast, the AC||Zn of the bare Zn anode showed a sudden drop in capacity after 1500 cycles. This drop might be caused by the dendrite piercing the fiberglass diaphragm. During the period of capacity decline, the CE of the AC||Zn battery decreased considerably. In addition, the AC||LIG-Zn battery can maintain 5000 stable cycles at a high current density of 5 A g<sup>-1</sup> (Fig. 7b). This result shows that the addition of LIG stabilizes the growth of dendrites and confers the battery with long-term cyclability.

Figure 7c shows the rate performance of the two batteries at different current densities. As expected, the specific capacity of the AC||LIG-Zn battery was higher than that of the AC||Zn battery at all rates. The capacity of the AC||LIG-Zn battery was 92.5, 80.7, 74.3, 66.4, 60.1, and 57.2 mAh g<sup>-1</sup> when tested at 0.2, 0.5, 1, 2, 5, and 10 A g<sup>-1</sup>, respectively. The mean overpotential values of the AC||Zn battery were 73.6, 65.8, 59.2, 54.2, 50.2, and 46.3 mV g<sup>-1</sup>. When the current returned to the previous value of 0.5 A g<sup>-1</sup>, the AC||LIG-Zn battery returned to the previous capacity (80.7 mAh g<sup>-1</sup>), indicating that the anode has excellent reversibility. Figure 7d shows the charge–discharge curve of the AC||LIG-Zn and AC||Zn batteries for the 2000th cycle at a current of 5 A g<sup>-1</sup>. The AC||LIG-Zn battery also shows higher charge–discharge specific capacity than the AC||Zn battery. To further investigate the fast Zn<sup>2+</sup> storage kinetics of the LIG-Zn electrode, the CV curve was examined over a scanning rate ranging from 10 to 100 mV s<sup>-1</sup> (Fig. 7e). All the CV curves present a nearly rectangular shape. The pseudocapacitive reactions related to the plating/stripping of the Zn/Zn<sup>2+</sup> process were indicated. The high reversibility of the entire charge transfer process was demonstrated, and the fast deposition kinetics of LIG-Zn was revealed [42, 43].

## 4 Conclusions

In conclusion, this study reported a novel method for manufacturing advanced Zn batteries. LIG was generated by a laser marking a PI film and applied to a 3D Zn anode. The results showed that the addition of LIG substantially reduced the nucleation overpotential and deposition potential of Zn compared with those of the bare Zn foil. After 3D structure treatment on the surface of the Zn foil, the specific surface area of the electrode sheet increased, and the conductivity and mechanical stability were considerably improved.

Electrochemical experiments prove that using LIG-Zn as an anode can substantially reduce the current density distribution and inhibit Zn dendrite formation. At the same time, LIG can release the residual stress of electroplating Zn so

that the plating process is uniform and dendrite-free. For example, the initial nucleation overpotential of the LIG-Zn anode is as low as 2.8 mV at 1 mA cm<sup>-2</sup>. The cycle life reaches 600 h when the areal capacity is 0.5 mAh cm<sup>-2</sup>. In addition, LIG-Zn||AC achieves a high areal capacity of 80 mAh g<sup>-1</sup> at 1 A g<sup>-1</sup> in a full battery with AC as the cathode. The LIG-Zn electrode with a periodic concave and convex pattern has hydrophilic and zincophilic properties, which can achieve complete electrolyte wetting and uniform electroplating/dissolution at different currents and capacities. In contrast, batteries with bare Zn anodes have only an initial discharge-specific capacity of 50.3 mAh g<sup>-1</sup>. The current work provides a novel, low-cost, and scalable method for stabilizing Zn anodes.

**Acknowledgements** This research is supported by the Natural Science Foundation of Tianjin, China (Nos. 22JCQNJC00630 and 21JCYBJC00620) and National Key R&D Program of China (No. 2021YFF0500200).

**Author contributions** All authors read and approved the final manuscript.

**Availability of data and materials** The authors declare that all data supporting the findings of this study are available within the article.

## Declarations

**Competing interests** The authors declare that they have no known competing financial interests or personal relationships that have appeared to influence the work reported in this paper.

**Open Access** This article is licensed under a Creative Commons Attribution 4.0 International License, which permits use, sharing, adaptation, distribution and reproduction in any medium or format, as long as you give appropriate credit to the original author(s) and the source, provide a link to the Creative Commons licence, and indicate if changes were made. The images or other third party material in this article are included in the article's Creative Commons licence, unless indicated otherwise in a credit line to the material. If material is not included in the article's Creative Commons licence and your intended use is not permitted by statutory regulation or exceeds the permitted use, you will need to obtain permission directly from the copyright holder. To view a copy of this licence, visit <http://creativecommons.org/licenses/by/4.0/>.

## References

- Zubi G, Dufo-Lopez R, Carvalho M, Pasaoglu G (2018) The lithium-ion battery: state of the art and future perspectives. *Renew Sustain Energy Rev* 89:292–308
- Wang M, Zhang F, Lee CS, Tang Y (2017) Low-cost metallic anode materials for high performance rechargeable batteries. *Adv Energy Mater* 7:1700536
- Yesibolati N, Unirov N, Koishybay A, Omarova M, Kurmanbayeva I, Zhang Y, Zhao Y, Bakenow Z (2015) High performance Zn/LiFePO<sub>4</sub> aqueous rechargeable battery for large-scale applications. *Electrochim Acta* 15:505–511
- Wu MJ, Zhang GX, Wu MH, Prakash J, Sun SH (2019) Rational design of multifunctional air electrodes for rechargeable Zn-Air

- batteries: recent progress and future perspectives. *Energy Storage Mater* 21:253–286
5. Lim MB, Lambert TN, Chalamala BR (2021) Rechargeable alkaline zinc-manganese oxide batteries for grid storage: mechanisms, challenges and developments. *Mater Sci Eng R-Rep* 143:100593
  6. Zhou W, Zhu D, He J, Li J, Chen H, Chen Y, Chao D (2020) A scalable top-down strategy toward practical metrics of Ni–Zn aqueous batteries with total energy densities of 165 Wh kg<sup>-1</sup> and 506 Wh L<sup>-1</sup>. *Energy Environ Sci* 13:4157–4167
  7. Zhao YW, Wang DH, Li XL, Yang Q, Guo Y, Mo FN, Li Q, Peng CX, Li HF, Zhi CY (2020) Initiating a reversible aqueous Zn/sulfur battery through a “Liquid Film.” *Adv Mater* 32:2003070
  8. Han C, Li W, Liu HK, Dou S, Wang J (2020) Principals and strategies for constructing a highly reversible zinc metal anode in aqueous batteries. *Nano Energy* 74:104523
  9. Fan W, Ding J, Ding J, Zheng Y, Song W, Lin J, Xiao C, Zhong C, Wang H, Hu W (2021) Identifying heteroatomic and defective sites in carbon with dual-ion adsorption capability for high energy and power zinc ion capacitor. *Nano-Micro Lett* 13:1–18
  10. Li C, Xie X, Liang S, Zhou J (2020) Issues and future perspective on zinc metal anode for rechargeable aqueous zinc-ion batteries. *Energy Environ Mater* 3:146–159
  11. Gür TM (2018) Review of electrical energy storage technologies, materials and systems: challenges and prospects for large-scale grid storage. *Energy Environ Sci* 11:2696–2767
  12. Hao J, Li X, Zeng X, Li D, Mao J, Guo Z (2020) Deeply understanding the Zn anode behavior and corresponding improvement strategies in different aqueous Zn based batteries. *Energy Environ Sci* 13:3917–3949
  13. Yuan L, Hao J, Kao CC, Wu C, Liu HK, Dou SX, Qiao SZ (2021) Regulation methods for the Zn/electrolyte interphase and the effectiveness evaluation in aqueous Zn-ion batteries. *Energy Environ Sci* 14:5669–5689
  14. Zhao K, Wang C, Yu Y, Yan M, Wei Q, He P, Dong Y, Zhang Z, Wang X, Mai L (2018) Ultrathin surface coating enables stabilized zinc metal anode. *Adv Mater Interfaces* 5:1800848
  15. Bayaguud A, Luo X, Fu YP, Zhu CB (2020) Cationic surfactant-type electrolyte additive enables three-dimensional dendrite-free zinc anode for stable zinc-ion batteries. *ACS Energy Lett* 5:3012–3020
  16. Yang Q, Guo Y, Yan B, Wang C, Liu Z, Huang Z, Wang Y, Li Y, Li H, Song L (2020) Hydrogen-substituted graphdiyne ion tunnels directing concentration redistribution for commercial-grade dendrite-free zinc anodes. *Adv Mater* 32:2001755
  17. Kang L, Cui M, Jiang F, Gao Y, Luo H, Liu J, Liang W, Zhi C (2018) Nanoporous CaCO<sub>3</sub> coatings enabled uniform Zn stripping/plating for long-life zinc rechargeable aqueous batteries. *Adv Energy Mater* 8:1801090
  18. Bozzini B, Mele C, Veneziano A, Sodini N, Lanzafame G, Taurino A, Mancini L (2020) Morphological evolution of Zn-sponge electrodes monitored by in situ X-ray computed microtomography. *ACS Appl Mater Interfaces* 3:4931–4940
  19. Shi X, Xu G, Liang S, Li C, Guo S, Xie X, Ma X, Zhou J (2019) Homogeneous deposition of zinc on three-dimensional porous copper foam as a superior zinc metal anode. *ACS Sustain Chem Eng* 7:17737–17746
  20. Kang Z, Wu CL, Dong LB, Liu WB, Mou J, Zhang JW, Chang ZW, Jiang BZ, Wang GX, Kang FY (2019) 3D porous copper skeleton supported zinc anode toward high capacity and long cycle life zinc ion batteries. *ACS Sustain Chem Eng* 3:3364–3371
  21. Zang ZG, Zeng XF, Wang M, Hu W, Liu CR, Tang XS (2017) Tunable photoluminescence of water-soluble AgInZnS-graphene oxide (GO) nanocomposites and their application in-vivo bioimaging. *Sens Actuat B Chem* 252:1179–1186
  22. Chen XF, Huang Y, Han XP, Zhang KC (2018) Synthesis of cobalt nanofibers @ nickel sulfide nanosheets hierarchical core-shell composites for anode materials of lithium-ion batteries. *Electrochim Acta* 284:418–426
  23. Zhang B, Liu Y, Wu X, Yang Y, Chang Z, Wen Z, Wu Y (2014) An aqueous rechargeable battery based on zinc anode and Na<sub>0.95</sub>MnO<sub>2</sub>. *Chem Commun* 50:1209–1211
  24. Lin J, Peng Z, Liu Y, Ruiz-Zepeda F, Ye R, Samuel EL, Yacaman MJ, Jakobson BI, Tour JM (2014) Laser-induced porous graphene films from commercial polymers. *Nat Commun* 5:5714
  25. Zhang JB, Ren MQ, Li YL, Tour JM (2018) In situ synthesis of efficient water oxidation catalysts in laser-induced graphene. *ACS Energy Lett* 3:677–683
  26. Zhang JB, Zhang CH, Sha JW, Fei HL, Li YL, Tour JM (2017) Efficient water-splitting electrodes based on laser-induced graphene. *ACS Appl Mater* 9:26840–26847
  27. El-Kady MF, Strong V, Dubin S, Kaner RB (2012) Laser scribing of high-performance and flexible graphene-based electrochemical capacitors. *Science* 335:1326–1330
  28. Tao LQ, Tian H, Liu Y, Ju ZY, Pang Y, Chen YQ, Wang DY, Tian XG, Yan JC, Deng NQ (2017) An intelligent artificial throat with sound-sensing ability based on laser induced graphene. *Nat Commun* 8:14579
  29. Yang ZG, Xu CW, Yan HH, Liu YW, Yue C, Zhang LY, Shui M, Hu F, Shu J (2021) Laser-induced graphene assisting self-conversion reaction for sulfur-free aqueous Cu-S battery. *Adv Funct* 31:2103893
  30. Guo R, Yue WB, An YM, Ren Y, Yan X (2014) Graphene-encapsulated porous carbon-ZnO composites as high-performance anode materials for Li-ion batteries. *Electrochim Acta* 135:161–167
  31. Xie XS, Liang SQ, Gao JW, Guo S, Guo JB, Wang C, Xu GY, Wu XW, Chen G, Zhou J (2020) Manipulating the ion-transfer kinetics and interface stability for high-performance zinc metal anodes. *Energy Environ Sci* 13:503–510
  32. Ye RQ, James DK, Tour JM (2019) Laser-induced graphene: from discovery to translation. *Adv Mater* 31:1803621
  33. Zhang Q, Luan J, Tang Y, Ji X, Wang H (2020) Interfacial design of dendrite-free zinc anodes for aqueous zinc-ion batteries. *Angew Chem Int Ed* 59:13180–13191
  34. Guo Y, Wang R, Cui C, Xiong R, Wei Y, Zhai T, Li H (2020) Shaping Li deposits from wild dendrites to regular crystals via the ferroelectric effect. *Nano Lett* 20:7680–7687
  35. Liu P, Hao H, Celio H, Cui J, Ren M, Wang Y, Dong H, Chowdhury AR, Hutter T, Perras FA (2021) Multifunctional separator allows stable cycling of potassium metal anodes and of potassium metal batteries. *Adv Mater* 34:2105855
  36. Xie F, Li H, Wang X, Zhi X, Chao D, Davey K, Qiao SZ (2021) Mechanism for zincophilic sites on zinc-metal anode hosts in aqueous batteries. *Adv Energy Mater* 11:2003419
  37. Liang P, Yi J, Liu X, Wu K, Wang Z, Cui J, Liu Y, Wang Y, Xia Y, Zhang J (2020) Highly reversible Zn anode enabled by controllable formation of nucleation sites for Zn-based batteries. *Adv Funct Mater* 30:1908528
  38. Yong JL, Chen F, Yang Q, Fang Y, Huo JL, Hou X (2015) Femtosecond laser induced hierarchical ZnO superhydrophobic surfaces with switchable wettability. *Chem Comm* 48:9813–9816
  39. Jia H, Qiu MH, Lan CT, Liu HQ, Dirican M, Fu SH, Zhang XW (2022) Advanced zinc anode with nitrogen-doping interface induced by plasma surface treatment. *Adv. Sci.* 9:2103952
  40. Zhou X, Cao P, Wei A, Zou A, Ye H, Liu W, Tang J, Yang J (2021) Driving the interfacial ion-transfer kinetics by mesoporous TiO<sub>2</sub> spheres for high-performance aqueous Zn-ion batteries. *ACS Appl Mater Interfaces* 13:8181–8190
  41. He H, Tong H, Song X, Song X, Liu J (2020) Highly stable Zn metal anodes enabled by atomic layer deposited Al<sub>2</sub>O<sub>3</sub> coating for aqueous zinc-ion batteries. *J Mater Chem A* 8:7836–7846

42. Zhou HT, Liu C, Wu JC, Liu MH, Zhang D, Song HL, Zhang XY, Gao HQ, Yang JH, Chen D (2019) Boosting the electrochemical performance through proton transfer for the Zn-ion hybrid supercapacitor with both ionic liquid and organic electrolytes. *J Mater Chem A* 16:9708–9715
43. Lu YY, Li ZW, Bai ZY, Mi HY, Ji CC, Pang H, Yu C, Qiu JS (2020) High energy-power Zn-ion hybrid supercapacitors enabled by layered B/N co-doped carbon cathode. *Nano Energy* 66:104132

**Publisher's note** Springer Nature remains neutral with regard to jurisdictional claims in published maps and institutional affiliations.



**Hui Xiao** received a master's degree from Tianjin University, Tianjin, China, in 2023. His major interests are energy storage devices and ultra-fast laser texturing technique.



**Chengjuan Yang** received a PhD degree from the Xi'an Jiaotong University, China, in 2013. She is currently an associate professor at the School of Mechanical Engineering at Tianjin University. Her major research interests focus on ultrafast laser micro/nano manufacturing technology and its application.



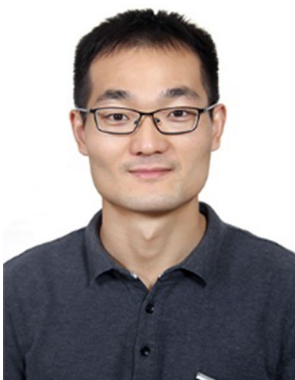
**Huimin Qi** is studying at the School of Mechanical Engineering of Tianjin University for a master's degree. She majored in mechanical engineering.



**Yuchun Tong** is studying for a master's degree at the School of Mechanical Engineering, Tianjin University. His major research interests focus on energy storage devices and ultrafast laser technology.



**Faze Chen** is a lecturer at the School of Mechanical Engineering, Tianjin University. He obtained a PhD in Mechanical Engineering from Dalian University of Technology, China, in 2018. His research interests focus on functional surfaces with liquid repellence, laser-based micro-additive/subtractive manufacturing, and atmospheric pressure cold plasmas.



**Zhen Yang** received a PhD degree from the University of Warwick, Coventry, UK, in 2021. He is currently an associate professor at the School of Mechanical Engineering at Tianjin University. His major research interests are laser micro/nano manufacturing, bio-inspired functional surfaces, and energy storage devices.